CFD Letters www.cfdl.issres.net Vol. 2 (4) – December 2010

Mixed Convection in a Lid-Driven Cavity Utilizing Nanofluids

M. Muthtamil Selvan[C]
Department of Mathematics, Anna University of Technology Tirunelveli, Tirunelveli, INDIA

Received: 02/09/2010 – Revised 17/12/2010 – Accepted 18/12/2010

Abstract

Heat transfer enhancement in a two-sided lid-driven cavity utilizing nanofluids is investigated for various pertinent parameters. A model is developed to analyze the behaviour of nanofluids taking into account the solid volume fraction χ. The top and bottom moving walls are maintained at different constant temperatures while the vertical walls are adiabatic. The numerical approach is based on the finite volume technique with a staggered grid arrangement. The SIMPLE algorithm is used for handling the pressure velocity coupling. Numerical solutions are obtained for wide range of parameters and copper water nanofluid is used with Pr=6.2. Numerical results show the inclusion of nanoparticles into the base fluid has produced an augmentation of the heat transfer coefficient, which has been found to increase appreciably with an increase of particles volume concentration. Detailed results are presented in the form of streamlines, isotherms and average Nusselt numbers.

Keywords: Nanofluid; Mixed convection; Lid-driven; Finite-volume method.

1. Introduction

Low thermal conductivity of convectional heat transfer fluids such as water, minerals oil and ethylene glycol have primary limitations in enhancing the performance of many industrial processes, including chemical production, power stations, transportation and microelectronics. To overcome this disadvantage there is a strong motivation to develop advanced heat transfer medium with substantially higher conductivity. Nanofluids are a new kind of heat transfer medium containing a small quantity of nanosized particles (usually less than 100nm) that are uniformly and stably suspended in a liquid.

Khanafer et al. [1] numerically investigated the heat transfer behavior of nanofluids in a two-dimensional horizontal enclosure. The nanofluids were assumed to be in single phase, in thermal equilibrium and without velocity slip between base fluid and particle. They found that the suspended nanoparticles substantially increase the heat transfer rate for any given Grashof number. More recently, Tiwari and Das [2] investigated numerically heat transfer augmentation in a lid-driven cavity filled with nanofluids. They found that the nanoparticles when immersed in a fluid are capable of increasing the heat transfer capacity of base fluid. As solid volume fraction increases, the effect is more pronounced. Koo and Kleinstreuer [3] discussed the effects of Brownian, thermo-

[C] Corresponding Author: M. Muthtamilselvan
Email: muthtamil1@yahoo.co.in Telephone: +91-461-2310044 Fax: +91-461-2310044

PII: S2180-1363(10)24163-X

phoretic and osmo-phoretic motions on the effective thermal conductivities. They found that the role of Brownian motion is much more important than the thermo-phoretic and osmo-phoretic motions. They suggested that a high-Prandtl number base fluid and a high aspect ratio channel should be used for better heat transfer performance. Furthermore, the particle interaction can be neglected when the nanofluid concentration is low (< 0.5%). Maiga et al. [4] presented a mathematical formulation and numerical method to determine the forced convective heat transfer and wall shear stress for the laminar and turbulent regions of water-Al_2O_3 and ethylene glycol-Al_2O_3 flowing inside a uniformly heated tube. The solid-liquid mixture takes a single-phase behaviour into account, so the slip velocity between the phases was neglected. Furthermore, the local thermal equilibrium of the mixture and symmetry in flow were considered. Recently, Jou and Tzeng [5] used Khanafer's model to analyze heat transfer performance of nanofluids inside an enclosure taking into account the solid particle dispersion.

Kim et al. [6] proposed an analytical investigation to describe the natural convective heat transfer of nanofluids by introducing a new factor f which included the effect of the ratio of thermal conductivity of nanoparticles to that of the base fluid, the shape factor of the particles, the volume fraction of nanoparticles, the ratio of density of nanoparticles to that of the base fluid and the ratio of heat capacity based on the volume of nanoparticles to that of the base fluid. The results showed that the heat transfer coefficients of nanofluid increased with increasing particle volume fraction.

The laminar flow forced convection heat transfer of Al_2O_3 water nanofluid inside a circular tube with constant wall temperature was investigated experimentally by Heris et al [7]. Their experimental results indicate that heat transfer coefficient of nanofluids increases with peclet number as well as nanoparticle concentration. Wen and Ding [8] have studied Al_2O_3 water nanofluid heat transfer in laminar flow under constant wall heat flux and reported an increase in nanofluid heat transfer coefficient with Reynolds number and nanoparticles concentration particularly at the entrance region. They expressed that thermal developing length for nanofluid was greater than pure water. The reason for heat transfer enhancement for nanofluids is the decreased thermal boundary layer thickness due to non-uniform distribution of thermal conductivity and viscosity resulting from Brownian motion of nanoparticles. Putra et al. [9] presented the experimental observations on the natural convection of two oxides (Al_2O_3 and CuO)-water based nanofluids inside a horizontal cylinder heated from one end and cooled from the other. The dependence of parameters such as particle concentration, particle material and geometry of the containing cylinder were investigated at steady-state conditions. For an up to date review of heat transfer in nanofluids one may refer to Das et al. [10] and Wang and Mujumdar [11].

Mixed convection in a lid-driven cavity flow problems are encountered in a variety of engineering applications including cooling of electronic devices, lubrication technologies and MEMS applications. Kuhlmann et al. [12] performed experimental and theoretical investigations into the two- and three-dimensional flows which are included when the two facing sides of the cavity move with constant velocities in directions opposite to each other. Maxwell's model [13] predicted that the effective thermal conductivity of suspensions containing spherical particles increases with an increase in the volume fraction of the solid particles. In the present study, mixed convection flow in a lid-driven square cavity filled with nanofluid is investigated numerically. The main objective of this study is to determine the effect of solid volume fraction on the heat transfer in the enclosure.

2. Mathematical analysis

2.1. Governing equations

Consider a steady-state two-dimensional square cavity filled with nanofluid of height H as shown in Fig. 1. It is assumed that the top wall is moving from left to right at a constant speed U_0 and is maintained at a constant temperature Tc. The bottom wall is maintained at a constant temperature Th (Th>Tc). Two different cases were considered as shown in Fig. 1. In case I, the bottom wall is moving from right to left. In case II, the bottom wall is moving from left to right.

The vertical sidewalls are considered to be adiabatic. The nanofluid in the enclosure is Newtonian, incompressible, and laminar. The nanoparticles are assumed to have uniform shape and size. Also, it is assumed that both the fluid phase and nanoparticles are in thermal equilibrium state and they flow at the same velocity. The physical properties of the nanofluid are considered to be constant expect the density variation in the body force term of the momentum equation which is satisfied by the Boussinesq's approximation. Under the above assumptions the system of equations governing the two dimensional motion of an nanofluid is

$$\frac{\partial u}{\partial x}+\frac{\partial v}{\partial y}=0 \tag{1}$$

$$u\frac{\partial u}{\partial x}+v\frac{\partial u}{\partial y}=-\frac{1}{\rho_{nf,0}}\frac{\partial p}{\partial x}+\frac{\mu_{eff}}{\rho_{nf,0}}\nabla^2 u \tag{2}$$

$$u\frac{\partial v}{\partial x}+v\frac{\partial v}{\partial y}=-\frac{1}{\rho_{nf,0}}\frac{\partial p}{\partial y}+\frac{\mu_{eff}}{\rho_{nf,0}}\nabla^2 v+\frac{1}{\rho_{nf,0}}\left[\chi\rho_{s,0}\beta_s+(1-\chi)\rho_{nf,0}\beta_f\right]g(\theta-\theta_c) \tag{3}$$

$$u\frac{\partial \theta}{\partial x}+v\frac{\partial \theta}{\partial y}=\alpha_{nf}\nabla^2\theta \tag{4}$$

where

$$\alpha_{nf}=\frac{K_{eff}}{\left(\rho C_p\right)_{nf,0}} \tag{5}$$

and the effective viscosity as given by Brinkman [14] as

$$\mu_{nf}=\frac{\mu_f}{(1-\chi)^{2.5}} \tag{6}$$

The effective density of the nanofluid at reference temperature is

$$\mu_{nf,0}=(1-\chi)\rho_{nf,0}+\chi\rho_{s,0} \tag{7}$$

and the heat capacitance of nanofluid is

$$\left(\rho C_p\right)_{nf}=(1-\chi)(\rho C_p)_f+\chi(\rho C_p)_s \tag{8}$$

as given by Xuan and Li [15]. The effective thermal conductivity of the solid-liquid mixture was introduced by Wasp [16] as follows

$$\frac{k_{eff}}{k_f}=\frac{(k_s+2k_f)-2\chi(k_f-k_s)}{(k_s+2k_f)+\chi(k_f-k_s)} \tag{9}$$

This equation is applicable for the two-phase mixture containing micro-sized particles. In the absence of any convenient formula, the calculation of effective thermal conductivity can be obtained from the above equation. Introducing the following dimensionless variables and parameters:

$$X=\frac{x}{H},\ Y=\frac{y}{H},\ U=\frac{u}{U_0},\ V=\frac{v}{U_0},\ T=\frac{\theta-\theta_c}{\theta_h-\theta_c}$$

$$Gr=\frac{g\beta\Delta\theta H^3}{{v_f}^2},\ P=\frac{p}{\rho {U_0}^2},\ \mathrm{Re}=\frac{U_0 H}{v_f},\ \mathrm{Pr}=\frac{v_f}{\alpha_f}$$

the governing equations (1)-(4) may be written in the dimensionless form as

$$\frac{\partial U}{\partial X}+\frac{\partial V}{\partial Y}=0 \tag{10}$$

$$U\frac{\partial U}{\partial X}+V\frac{\partial U}{\partial Y}=-\frac{\rho_{f,0}}{\rho_{nf,0}}\frac{\partial P}{\partial X}+\frac{1}{\mathrm{Re}}\frac{\mu_{eff}}{v_f\rho_{nf,0}}\nabla^2 U \tag{11}$$

$$U\frac{\partial V}{\partial X}+V\frac{\partial V}{\partial Y}=-\frac{\rho_{f,0}}{\rho_{nf,0}}\frac{\partial P}{\partial Y}+\frac{1}{\mathrm{Re}}\frac{\mu_{eff}}{v_f\rho_{nf,0}}\nabla^2 V+\frac{\left[\chi\rho_{s,0}\beta_s+(1-\chi)\rho_f\beta_f\right]}{\rho_{nf,0}\beta_f}RiT \tag{12}$$

$$U\frac{\partial T}{\partial X}+V\frac{\partial T}{\partial Y}=\frac{\alpha_{nf}}{\alpha_f}\frac{1}{\Pr.\mathrm{Re}}\nabla^2 T \tag{13}$$

The dimensionless boundary conditions, used to solve equations (10) to (13) are as follows.

$$U=1,\ V=0,\ T=0\ (Y=1)$$

$$U=-1\ (Case\ I),\ U=1(CaseII),\ V=0,\ T=1(Y=0)$$

$$U=V=0,\ \frac{\partial T}{\partial X}=0\ (X=0,\ 1)$$

The governing equations (11) − (13) can be written for a general field variable ϕ as

$$\frac{\partial}{\partial X}(U\phi)+\frac{\partial}{\partial Y}(V\phi)=\frac{\partial}{\partial X}\left(\Gamma^{\phi}\frac{\partial \phi}{\partial X}\right)+\frac{\partial}{\partial Y}\left(\Gamma^{\phi}\frac{\partial \phi}{\partial Y}\right)+S^{\phi} \tag{14}$$

where ϕ is the dependent variable, Γ^{ϕ} is the diffusion coefficient and S^{ϕ} is the source term. The momentum equation in the X direction is obtained when

$$\phi=U,\ \Gamma^{\phi}=\frac{1}{\mathrm{Re}}\frac{\mu_{eff}}{\nu_f\rho_{nf,0}},\ S^{\phi}=-\frac{\partial P}{\partial X}\frac{\rho_{f,0}}{\rho_{nf,0}}$$

the Y direction is obtained when

$$\phi=V,\ \Gamma^{\phi}=\frac{1}{\mathrm{Re}}\frac{\mu_{eff}}{\nu_f\rho_{nf,0}},\ S^{\phi}=-\frac{\rho_{f,0}}{\rho_{nf,0}}\frac{\partial P}{\partial Y}+\nabla^2 V+\frac{\left\lfloor\chi\rho_{s,0}\beta_s+(1-\chi)\rho_f\beta_f\right\rfloor}{\rho_{nf,0}\beta_f}RiT$$

and the energy equation is obtained when

$$\phi=T,\ \Gamma^{\phi}=\frac{\alpha_{nf}}{\alpha_f}\frac{1}{\Pr.\mathrm{Re}},\ S^{\phi}=0$$

The average Nusselt number can be expressed as

$$Nu_{avg}=-\frac{k_{eff}}{k_f}\int_0^1\frac{\partial T}{\partial Y}dX\ .$$

2.2 Method of solution

Numerical solutions to the governing equations are secured by employing the finite volume computational procedure using staggered grid arrangement with the SIMPLE algorithm as given in Patankar [17]. The convective terms in the interior points are discretized by using the deferred QUICK scheme [18] and central difference scheme was used adjacent to the boundaries. The resulting algebraic equations are solved by using tridiagonal matrix (TDMA) algorithm. The pseudo-transient approach is followed for the numerical solution as it is useful for situation in which the governing equations give rise to stability problems, e.g., buoyant flows [19]. Euclidean norm of the residual is taken as convergence criteria for each dependent variable in the entire row field [20]. The iteration is carried out until the normalized residuals of the mass, momentum and temperature equation become less than 10^{-7}.

2.3 Grid independence study and code validation

In the present study the grid independent test is conducted for χ = 0% and Ri = 1. This test is performed using successively sized grids, from 11 × 11, 21 × 21, 41 × 41, 81 × 81 and 161 × 161. It can be seen from Fig. 2 that the average Nusselt number remains almost the same for grids finer than 81 × 81 and heavily depends on the grid size for less finer grids. Therefore considering both the accuracy and the computational time involved computations were performed with 81 × 81 grid.

The validation of the present computational code has been verified for Rayleigh numbers between 10^3 to 10^6. Table 1 compares the results with those by de Vahl Davis [21], Manzari [22] and Wan et al. [23]. The computed results are in very good agreement with the benchmark

solution. There is not much experimental data available in the literature for heat transfer within square cavities using nanofluids. The problem of laminar natural convection in a square cavity using nanofluids has been solved and compared the results with those Santra et al. [24]. They considered the left wall with hot temperature and the right wall with cold temperature. The top and bottom walls are insulated. Fig. 3 shows that the average Nusselt number for the present results and Santra et al. [24]. This comparison shows a good agreement between the two numerical results. This in effect provided credence to the accuracies of the present numerical solutions.

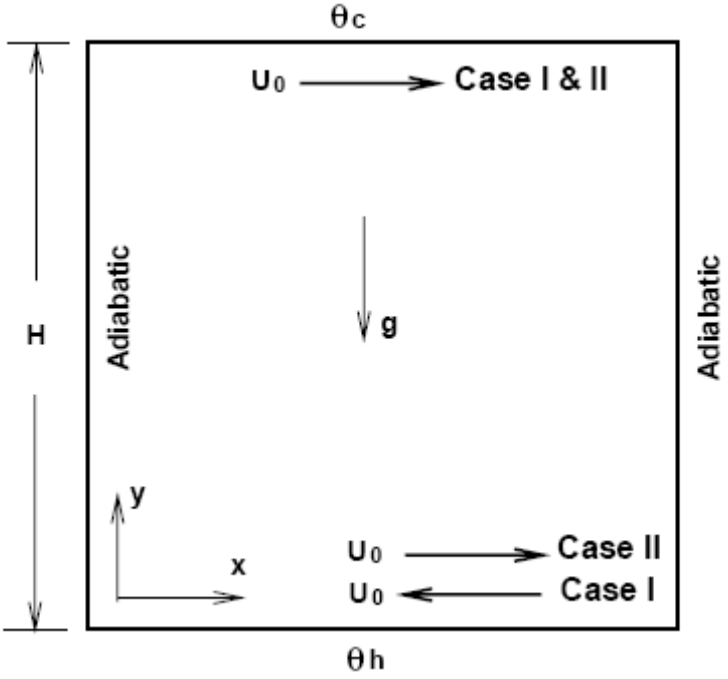

Figure 1: Flow configuration and coordinate system for two cases.

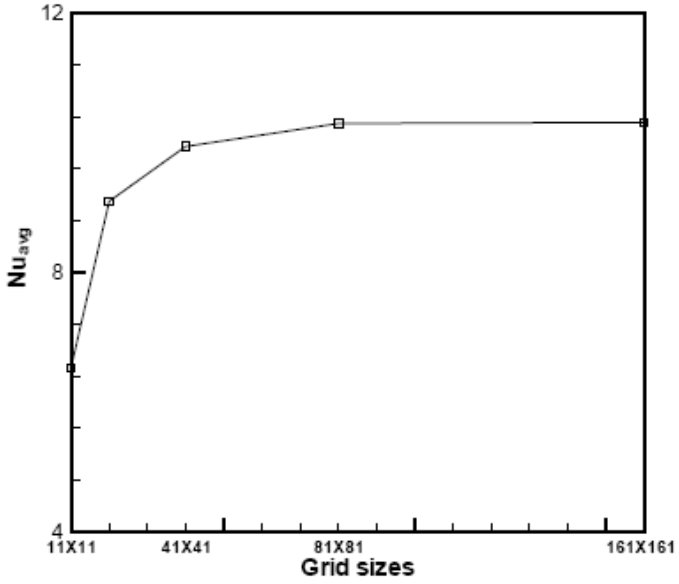

Figure 2: Average Nusselt number for different mesh sizes at $\chi = 0.0\%$ and $Ri = 1$.

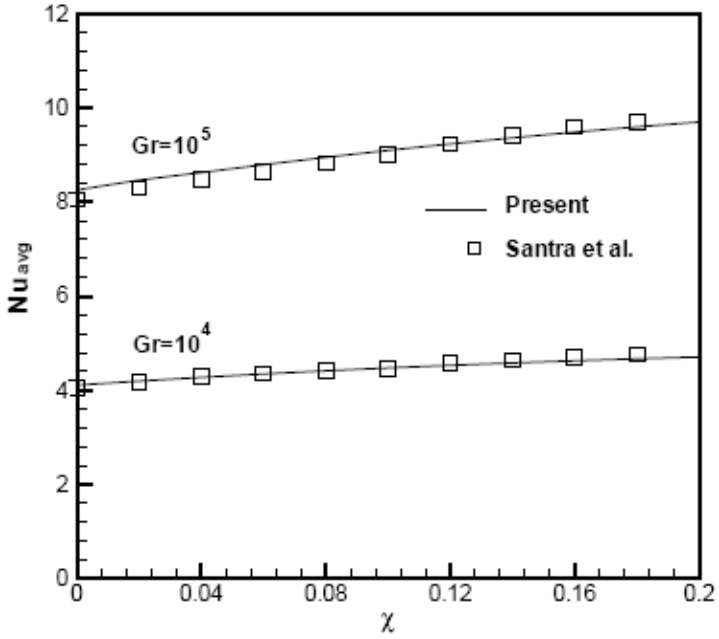

Figure 3: Validation of the present code with the results of Santra et al. [24].

TABLE 1: COMPARISON OF NUSSELT NUMBER (NU) AND THE CORRESPONDING ORDINATE (MAX., MAXIMUM; MIN., MINIMUM; AV., AVERAGE)

Ra	Nu	Ref. [21]	Ref. [22]	Ref. [23]	Present study
10^2	Max.	1.50	1.47	1.501	1.508
		(0.092)	(0.109)	(0.08)	(0.094)
	Min.	0.692	0.623	0.691	0.69
		(1.0)	(1.0)	(1.0)	(1.0)
	Av.	1.12	1.074	1.117	1.118
10^4	Max.	3.53	3.47	3.579	3.545
		(0.143)	(0.125)	(0.13)	(0.145)
	Min.	0.586	0.497	0.577	0.582
		(1.0)	(1.0)	(1.0)	(1.0)
	Av.	2.243	2.084	2.254	2.248
10^5	Max.	7.71	7.71	7.945	7.833
		(0.08)	(0.08)	(0.08)	(0.08)
	Min.	0.729	0.614	0.698	0.721
		(1.0)	(1.0)	(1.0)	(1.0)
	Av.	4.52	4.3	4.598	4.546
10^6	Max.	17.92	17.46	17.86	18.642
		(0.038)	(0.039)	(0.03)	(0.031)
	Min.	0.989	0.716	0.9132	0.9959
		(1.0)	(1.0)	(1.0)	(1.0)
	Av.	8.8	8.743	8.976	8.975

3. Results and discussion

The numerical code developed in the present investigation is used to carry out a number of simulations for a wide range of controlling parameters of Ri and χ . The parameters are varied in the following ranges: the solid volume fraction from 0% to 8% and the Richardson number from 10^{-2} to 16 by varying the Reynolds number while the Grashof number is fixed at 10^4. The working fluid is chosen as nanofluid with Prandtl number 6.2. The thermophysical properties of fluid and solid phase were given by Khanafer et al. [1]. Two different cases are considered according to the motion of the horizontal walls.

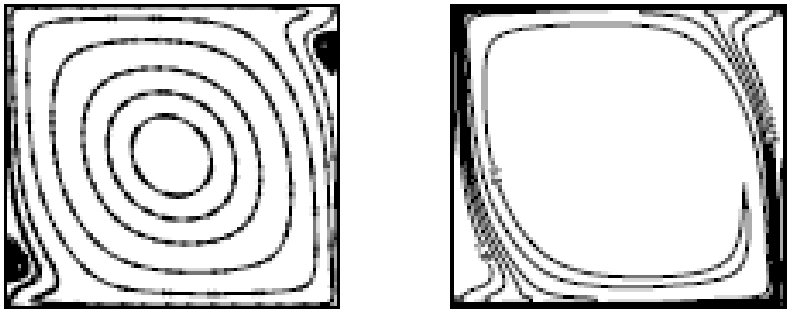

(*a*) $\chi = 0\%$

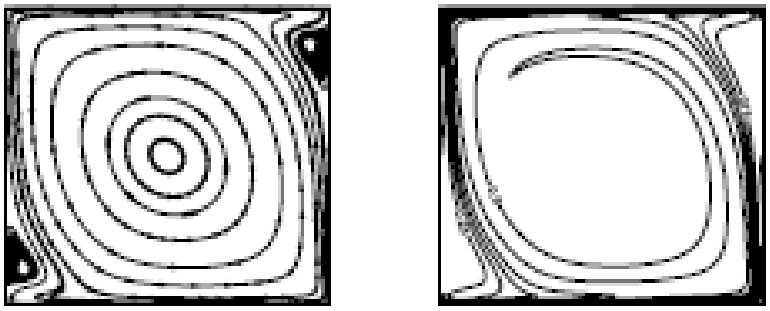

(*b*) $\chi = 8\%$

Figure 4: Streamlines (on the left) and isotherms (on the right) for case I at $Ri = 1 \times 10^{-2}$.

Case I: In this case the top wall is moving from left to right and bottom wall is moving from right to left. The streamlines (on the left) and isotherms (on the right) for Ri = 10^{-2} to 16 are shown in Figs. 4-6. For Ri = 10^{-2}, streamlines show that the forced convection plays a dominant role and recirculation flow is mostly generated by the moving lids (Fig. 4). The main circulation fills the entire cavity and minor cells are visible near the left bottom and right top corners. The isotherms are clustered close to the bottom and top lids. As χ increases from 0% to 8% the thickness of the boundary layer is reduced and the convection mode of heat transfer is enhanced. The increase in χ does not reflect on the streamlines in the cavity which demonstrates that the contribution of buoyancy in the flow development is insignificant for Ri = 10^{-2}.

For Ri = 1, streamlines show that the minor cells disappear and the major cell fills in the entire cavity (Fig. 5), because, the speed of the lid is decreased and buoyancy effect is increased. In this case mixed convection is more dominating within the enclosure. When Ri = 16, in Fig. 6, the effect of natural convection is far more compared to forced convection effect. For this case, conditions are strongly favoring the phenomena of natural convection. The increase in χ reduced the thickness of the thermal boundary layer as seen in the Fig. 6. For case I, the effect of nanoparticles is not much. Thus the streamlines and isotherms show a similar trend for the range of χ from 0% to 8%.

Case II: The streamlines and isotherms in the cavity for Ri = 10^{-2} − 16 and for different values of χ are presented in Figs. 7-9. In Fig. 7, streamlines show that two major cells rotating at the top and bottom of the enclosure and minor cells visible near the right middle vertical wall. This behavior is very logical because the forced convection is dominant and buoyancy force is negligible. Isotherms for this case indicates that the colder fluid occupies top half of the cavity and hotter fluid occupies bottom half of the cavity. In this case fluid particles are not well mixed compared to case I for Ri = 10^{-2}. As Richardson number is increased to 1, streamlines show that the minor cells disappear and two major cells are rotating in counter clockwise directions. In this case, for four ranges of the volume fraction mixed convection mode dominates in the enclosure (Fig. 8). For Ri = 16, as χ increases in Fig. 9, the isotherms crowded in the middle of the cavity spread out to the top and bottom, indicating that natural convection is dominating.

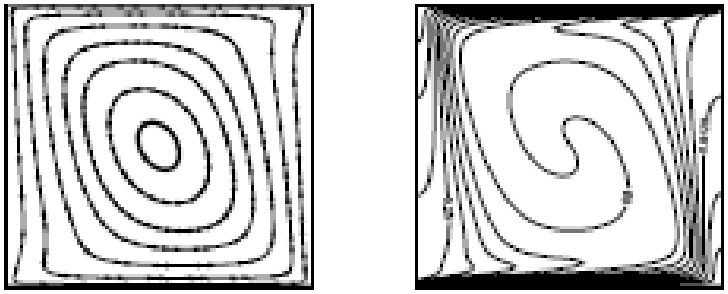

(*a*) $\chi = 0\%$

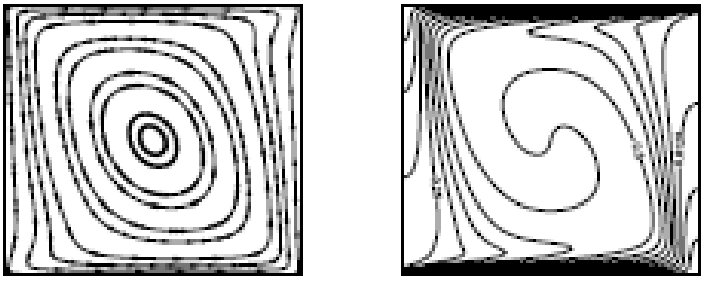

(*b*) $\chi = 8\%$

Figure 5: Streamlines (on the left) and isotherms (on the right) for case I at $Ri = 1$.

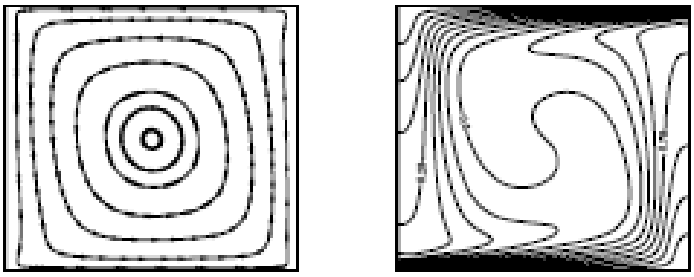

(*a*) $\chi = 0\%$

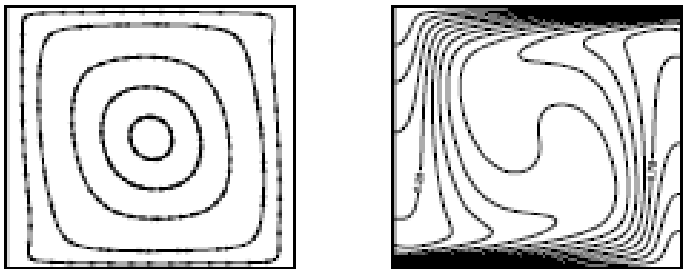

(*b*) $\chi = 8\%$

Figure 6: Streamlines (on the left) and isotherms (on the right) for case I at $Ri = 16$.

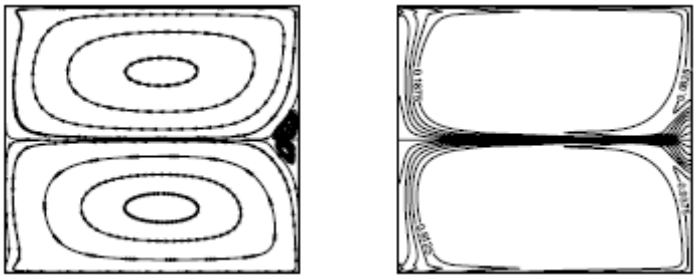

(a) $\chi = 0\%$

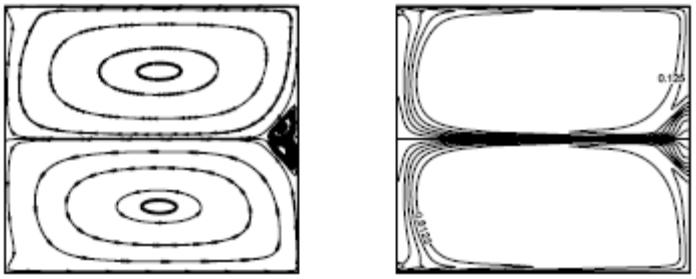

(b) $\chi = 8\%$

Figure 7: Streamlines (on the left) and isotherms (on the right) for case II at $Ri = 1 \times 10^{-2}$.

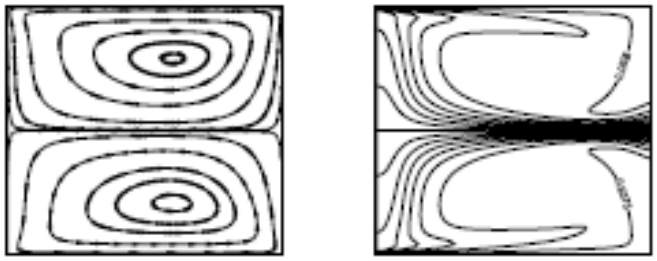

(a) $\chi = 0\%$

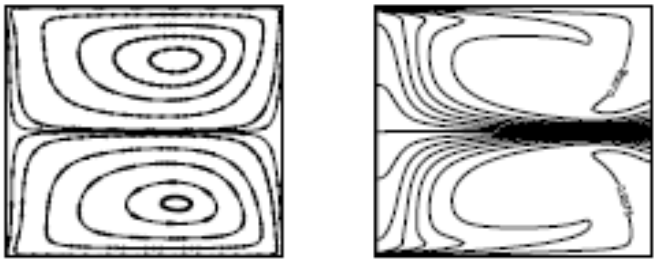

(b) $\chi = 8\%$

Figure 8: Streamlines (on the left) and isotherms (on the right) for case II at $Ri = 1$.

The velocity profiles at mid-section of the cavity for various range of solid volume fraction for the two cases are displayed in Fig. 10. It can be seen that the nanofluid does not have appreciable effect on the flow field for both cases. Finally, the average Nusselt number for two cases at different values of solid volume fractions are displayed in Fig. 9. It is observed that for fixed value of the Richardson number, the average Nusselt number increases with increasing value of the volume fraction. The rate of heat transfer is maximum for $Ri = 10^{-2}$ and minimum for $Ri = 16$ in both cases. Also this figure shows a linear variation of the average Nusselt number with the solid volume fraction for both cases. The variations of the average Nusselt number for both cases are shown in Table 2. It should be noted that, when χ is 2%, the increase is approximately 2% for case I and 3% for case II. When χ is 4%, the increase is approximately 4% for case I and 6% for case II. When χ is 6%, the increase is approximately 6% for case I and 9% for case II. When χ is 8%, the increase is approximately 8% for case I and 11% for case II.

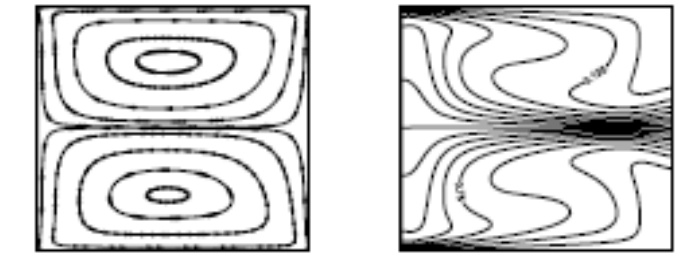

(*a*) $\chi = 0\%$

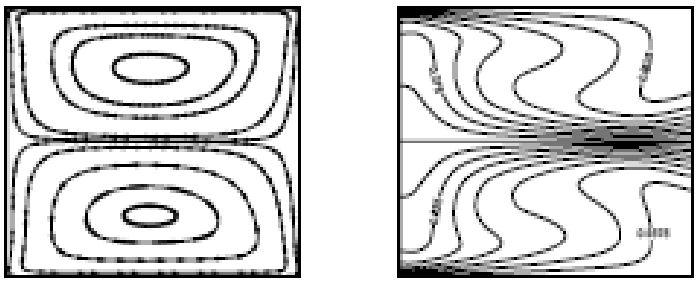

(*b*) $\chi = 8\%$

Figure 9: Streamlines (on the left) and isotherms (on the right) for case II at *Ri* = 16.

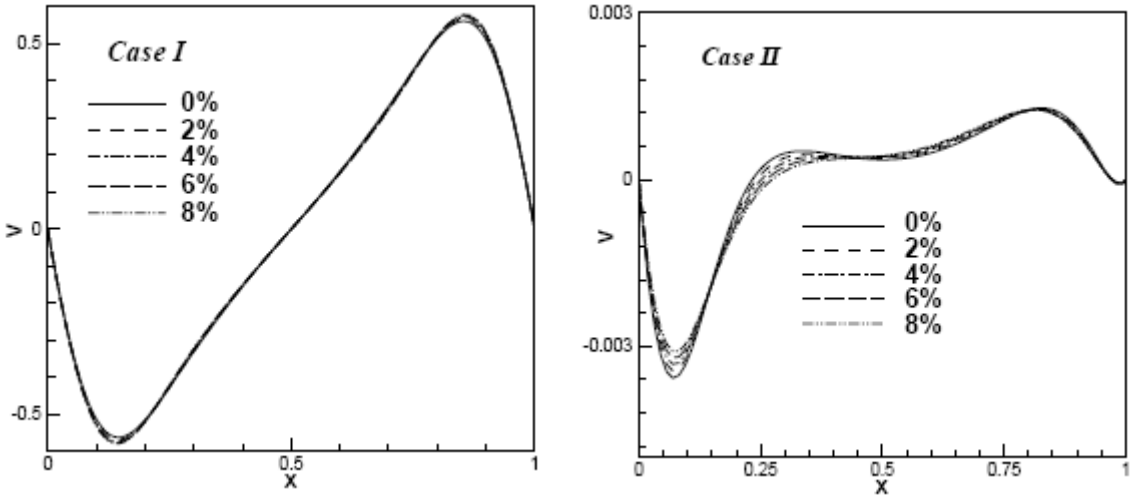

Figure 10: Velocity profiles at mid-plane of the cavity.

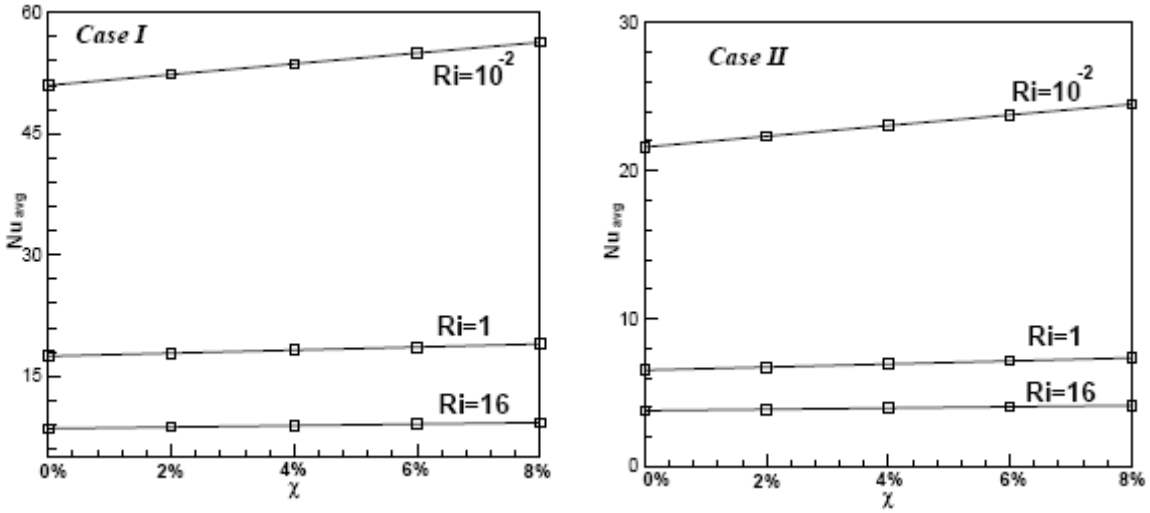

Figure 11: Average Nusselt number for two cases.

TABLE 2: COMPARISON OF THE AVERAGE NUSSELT NUMBER NU_{AVG} FOR TWO CASES AND VARIOUS SOLID VOLUME FRACTIONS

Ri	A	B	% increase[a]	D	% increase[b]	E	% increase[c]	F	% increase[d]
Case I									
10^{-2}	51.0	52.33	2.6	53.66	5.22	54.99	7.82	56.32	10.43
1	17.47	17.84	2.11	18.22	4.29	18.6	6.47	18.98	8.64
16	8.51	8.70	2.23	8.88	4.35	9.07	6.58	9.25	8.7
Case II									
10^{-2}	21.59	22.33	3.43	23.05	6.76	23.76	10.05	24.49	13.43
1	6.54	6.74	3.06	6.95	6.27	7.15	9.33	7.36	12.54
16	3.80	3.89	2.37	3.98	4.74	4.07	7.11	4.15	9.21

[a] $\frac{B-A}{A}\times 100$ [b] $\frac{D-A}{A}\times 100$ [c] $\frac{E-A}{A}\times 100$ [d] $\frac{F-A}{A}\times 100$

4. Conclusions

The flow and heat transfer is investigated in a bottom heated lid-driven square cavity filled with nanofluids. Two cases were considered depending on the direction of the moving walls. The major findings in this paper are:

- Heat transfer coefficient of nanofluids increases with increasing value of the nanoparticles concentration.
- The variation of the average Nusselt number is linear with solid volume fraction.
- The presence of nanoparticles in the fluid fails to produce appreciable effect on the flow field for both cases.
- For Ri = 10^{-2} and χ = 8%, the increase in rate of heat transfer is 13% in case II.

Nomenclature

g	gravitational acceleration
Gr	Grashof number
H	enclosure length
k_f	thermal conductivity of the fluid
k_s	thermal conductivity of the solid
Nu_{avg}	average Nusslet number
P	Pressure
Pr	Prandtl number
Re	Reynolds number
Ri	Richardson number
T	dimensionless temperature
U,V	dimensionless velocities in X- and Y-direction respectively
U_0	lid velocity
U_c	dimensionless velocity in X-direction at mid-plane of the cavity
u,v	velocities in x- and y-direction respectively
V_c	dimensionless velocity in Y-direction at mid-plane of the cavity
X,Y	dimensionless Cartesian coordinates
x,y	Cartesian coordinates
Greek symbols	
α	effective thermal diffusivity
β_f	coefficient of thermal expansion of fluid
$\Delta\theta$	temperature difference
θ	temperature
μ	effective dynamic viscosity

υ	effective kinematic viscosity
ρ	fluid density
χ	solid volume fraction

Subscripts

avg	average
c	cold wall
eff	effective
f	fluid
h	hot wall
nf	nanofluid
s	solid

References

[1] Khanafer, K., Vafai, K., Lightstone, M. Buoyancy driven heat transfer enhancement in a two- dimensional enclosure utilizing nanofluids. Int. J. Heat Mass Transfer, 2003. 46: p. 3639-3653.

[2] Tiwari, R.K., Das M.K., Heat transfer augmentation in a two-sided lid-driven differentially heated square cavity utilizing nanofluids. Int. J. Heat Mass Transfer, 2007. 50: p. 2002-2018.

[3] Koo, J., Kleinstreuer, C. Laminar nanofluid flow in microheat-sinks, Int. J. Heat Mass Transfer. 2005. 48: p. 2652-2661.

[4] Maiga, S.E.B., Nguyen, C.T., Galanis, N., Roy, G. Heat transfer behaviors of nanofluids in a uniformly heated tube. Superlattices Microstructures, 2004. 35: p. 543-557.

[5] Jou, R-Y., Tzeng, S-C. Numerical research on nature convective heat transfer enhancement filled with nanofluids in rectangular enclosures. Int. Comm. Heat Mass Transfer, 2006. 33: p. 727-736.

[6] Kim, J., Kang, Y.T., Choi, C.K. Analysis of convective instability and heat transfer characteristics of nanofluids. Phy. Fluids, 2004. 16: p. 2395-2401.

[7] Heris, S.Z., Esfahany, M.N., Etemad, S.Gh. Experimental investigation of convective heat transfer of Al_2O_3/water nanofluid in circular tube. Int. J. Heat Fluid Flow, 2007. 28: p. 203-210.

[8] Wen, D., Ding, Y. Experimental investigation into convective heat transfer of nanofluid at the entrance rejoin under laminar flow conditions. Int. J. Heat Mass Transfer, 2004. 47: p. 5181-5188.

[9] Putra, N., Roetzel, W., Das, S.K. Natural convection of nano-fluids. Heat Mass Transfer, 2003. 39: p. 775-784.

[10] Das, S.K., Choi, S.U.S., Patel, H.E. Heat transfer in nanofluids-a review. Heat Transfer Eng., 2006. 27: p. 3-19.

[11] Wang, X-Q., Mujumdar, A.S. Heat transfer characteristics of nanofluids: a review. Int. J. Thermal Sci., 2007. 46: p. 1-19.

[12] Kuhlmann, H.C., Wanschura, M., Rath, H.J. Elliptic instability in two-sided lid-driven cavity flow. European J. Mechanics B/Fluids, 1998. 17: p. 561-569.

[13] Maxwell, J.C. A Treatise on Electricity and Magnetism (second ed.), Oxford University Press, Cambridge 1904. p. 435-441.

[14] Brinkman, H.C. The viscosity of concentrated suspensions and solutions. J. Chemical Physics, 1952. 20: p. 571-581.

[15] Xuan, Y., Li, Q. Investigation on convective heat transfer and flow features of nanofluids. ASME J. Heat Transfer, 2003. 125: p. 151-155.

[16] Wasap, F.J. Solid-liquid slurry pipeline transportation, Trans. Tech.: Berlin 1977.

[17] Patankar, S.V. Numerical Heat Transfer and Fluid Flow, Hemisphere, Washington, DC, 1980.
[18] Hayase, T., Humphrey, J.A.C., Grief, R. A consistently formulated QUICK scheme for fast and stable convergence using finite-volume iterative procedures. J. Comp. Physics, 1992. 98: p. 108-118.
[19] Versteeg, H.K., Malalasekera, W. An Introduction to Computational Fluid Dynamics: the Finite Volume Method, Longman Group Ltd. 9 Malaysia, 1995.
[20] Van Doormaal, J.P., Raithby, G.D. Enhancements of the SIMPLE method for predicting incompressible fluid flows. Numerical Heat Transfer: Part A, 1984. 7: p. 207-163.
[21] Vahl Davis, D. de Natural convection of air in a square cavity: A bench mark solution. Int. J. Numer. Methods in Fluids, 1983. 3: p. 249-264.
[22] Manzari, M.T. An explicit finite element algorithm for convective heat transfer problems. Int. J. Numer. Methods for Heat and Fluid Flow, 1999. 9: p. 860-877.
[23] Wan, D.C., Patnaik, B.S.V., Wei, G.W. A new benchmark quality solution for the buoyancy-driven cavity by discrete singular convoluton. Numerical Heat Transfer: Part B, 2001. 40: p. 199-228.
[24] Santra, A.K., Sen, S., Chakraborty, N. Analysis of laminar natural convection in a square cavity using nanofluid, in: 31st National Conference on FMFP, Jadavpur University Kolkata, December, 2004. p. 240-248.